

Susceptibility weighted imaging: differentiating between calcification and hemosiderin*

Imagem ponderada em suscetibilidade magnética: diferenciando calcificação de hemossiderina

Jeam Haroldo Oliveira Barbosa¹, Antonio Carlos Santos², Carlos Ernesto Garrido Salmon³

Barbosa JHO, Santos AC, Salmon CEG. Susceptibility weighted imaging: differentiating between calcification and hemosiderin. Radiol Bras. 2015 Mar/Abr;48(2):93–100.

Abstract Objective: To present a detailed explanation on the processing of magnetic susceptibility weighted imaging (SWI), demonstrating the effects of echo time and sensitive mask on the differentiation between calcification and hemosiderin.

Materials and Methods: Computed tomography and magnetic resonance (magnitude and phase) images of six patients (age range 41–54 years; four men) were retrospectively selected. The SWI images processing was performed using the Matlab's own routine.

Results: Four out of the six patients showed calcifications at computed tomography images and their SWI images demonstrated hyperintense signal at the calcification regions. The other patients did not show any calcifications at computed tomography, and SWI revealed the presence of hemosiderin deposits with hypointense signal.

Conclusion: The selection of echo time and of the mask may change all the information on SWI images, and compromise the diagnostic reliability. Amongst the possible masks, the authors highlight that the sigmoid mask allows for contrasting calcifications and hemosiderin on a single SWI image.

Keywords: SWI; Magnetic resonance imaging; Magnetic susceptibility; Calcification; Hemosiderin.

Resumo Objetivo: Expor em detalhes o processamento da imagem ponderada em suscetibilidade magnética (*susceptibility weighted imaging* – SWI), destacando o efeito da escolha do tempo de eco e da máscara sensível à diferenciação de calcificação e hemossiderina simultaneamente.

Materiais e Métodos: Imagens de tomografia computadorizada e por ressonância magnética (magnitude e fase) foram selecionadas, retrospectivamente, de seis pacientes (idades entre 41 e 54 anos; quatro homens). O processamento das imagens SWI foi realizado em rotina própria no programa Matlab.

Resultados: Dos seis pacientes estudados, quatro apresentaram calcificações nas imagens de tomografia computadorizada. Nestes, as imagens SWI mostraram sinal hiperintenso para as regiões de calcificações. Os outros dois pacientes não apresentaram calcificações nas imagens de tomografia computadorizada e apresentaram depósito de hemossiderina com sinal hipointenso na imagem SWI.

Conclusão: A escolha do tempo de eco e da máscara pode alterar toda a informação da imagem SWI e comprometer a confiabilidade diagnóstica. Dentre as possíveis máscaras, destacamos que a máscara sigmoide permite contrastar calcificação e hemossiderina em uma única imagem SWI.

Unitermos: SWI; Ressonância magnética; Suscetibilidade magnética; Calcificação; Hemossiderina.

INTRODUCTION

In the clinical practice, the most frequently utilized magnetic resonance imaging modality is fundamentally weighted by relaxation time of tissues. At these images, the contrast is

based on the significant differences between transverse relaxation (T2) and/or longitudinal relaxation (T1) in the study region. However, relaxometry-weighted images cannot differentiate between hemosiderin and calcifications since both reduce the relaxation times due to inhomogeneity of the magnetic field generated by paramagnetic and diamagnetic atoms, respectively. On the other hand, susceptibility-weighted imaging (SWI) enhances the contrast of calcifications and hemosiderin deposits^(1,2). Thus, SWI has supplemented the clinical diagnosis of neurological disorders (cranioencephalic trauma and harmful clots), hemorrhagic disorders (vascular malformation, cerebral infarction and neoplasias) and neuroinfectious conditions (neurotoxoplasmosis and neurocysticercosis)⁽³⁾.

The SWI is generated by means of multiplication of magnitude image by a mask with values between 0 and 1 obtained from the phase image. Both images are generally acquired with a conventional clinical gradient echo (GE) sequence

* Study developed at Universidade de São Paulo – Programa de Pós-Graduação em Física Aplicada a Medicina e Biologia, Ribeirão Preto, SP, Brazil. Financial support: Fundação de Amparo à Pesquisa do Estado de São Paulo (Fapesp), Conselho Nacional de Desenvolvimento Científico e Tecnológico (CNPq) and Coordenação de Aperfeiçoamento de Pessoal de Nível Superior (Capes).

1. Master, Fellow PhD degree, Faculdade de Filosofia, Ciências e Letras de Ribeirão Preto da Universidade de São Paulo (FFCLRP-USP), Ribeirão Preto, SP, Brazil.

2. PhD, Professor, Faculdade de Medicina de Ribeirão Preto da Universidade de São Paulo (FMRP-USP), Ribeirão Preto, SP, Brazil.

3. PhD, Professor, Faculdade de Filosofia, Ciências e Letras de Ribeirão Preto da Universidade de São Paulo (FFCLRP-USP), Ribeirão Preto, SP, Brazil.

Mailing Address: Jeam Haroldo Oliveira Barbosa. Faculdade de Filosofia, Ciências e Letras de Ribeirão Preto – Universidade de São Paulo. Avenida Bandeirantes, 3900, Monte Alegre. Ribeirão Preto, SP, Brasil, 14040-901. E-mail: jeamharoldo@hotmail.com.

Received February 18, 2014. Accepted after revision August 5, 2014.

with appropriate echo time (TE)⁽⁴⁾. The main information on the susceptibility distribution (χ) on the SWI is on the phase image where the phase (ϕ) in a determined position (r) and with a certain TE is approximately:

$$\phi(r, TE) = \gamma * \chi(r) * B_0 * TE \quad (1)$$

where: γ is the gyromagnetic ratio of the hydrogen nucleus. If the phase of the nuclei of water molecules contained in the greatest part of the healthy brain tissue is considered as a reference phase, the equation 1 can be expressed in terms of phase difference:

$$\Delta\phi(r, TE) = \gamma * \Delta\chi(r) * B_0 * TE \quad (2)$$

where: $\Delta\chi(r)$ represents the difference of $\chi_{\text{tissue}} - \chi_{\text{water}}$. Thus, for relatively short echo times, such phase variation assumes values between 0 and $+\pi$ for paramagnetic tissue ($\Delta\chi > 0$) and $-\pi$ to 0 for diamagnetic tissue ($\Delta\chi < 0$). The change in the signal in both cases may be explained by the magnetic properties of the iron and calcium atoms. The authors highlight that the above descriptions consider the “left-hand” reference system, which defines the 0 intensity on the phase image as π , and the intensity 4095 as $-\pi$. On the other hand, the “right-hand” system defines such an interval as the contrary ($-\pi$ to π). Each manufacturer adopts a reference system. In order to find out the reference system one has only to observe the phase values of the blood vessels and basal ganglia, which are paramagnetic.

Although SWI is already a recognized technique, computed tomography (CT) is still considered to be a conclusive technique in the differential diagnosis of cerebral calcification⁽²⁾. Besides the already known economic factors related to CT and MRI, the authors consider that a more extensive utilization of SWI as a conclusive technique for the mentioned diagnosis is affected by two extremely important choices in the correct use of this technique, namely, the TE value in the images acquisition and the type of mask in the postprocessing phase. Such two choices influence the magnetic susceptibility contrast on the SWI. It is difficult to interpret the effects of such parameters because of the phase limitation to values within the interval $-\pi$ to $+\pi$. As the value of the tissue phase exceeds the π scale for long TE, the image phase assumes the added value of -2π . Such effect is called wrapping⁽⁵⁾. The incorrect selection of TE may lead to erroneous definition of the magnetic susceptibility contrast on the SWI.

The present study describes in detail the SWI processing, highlighting the effect of the selection of the TE and of

the sensitive mask to differentiate between calcification and hemosiderin, simultaneously in six patients with different diagnostic hypotheses. Additionally, the authors evaluated the effectiveness of this procedure, considering CT as the gold standard.

MATERIALS AND METHODS

Subjects

Six patients (four men and two women; age range between 41 and 54 years) were selected to illustrate the application of SWI as well the technique validity. The retrospective selection was made after the images acquisition, according to the following criteria: a) diagnostic suspicion of neurotoxoplasmosis, ventricular cysts and hemosiderin deposition; b) neurological CT and MRI studies at an interval of at least 3 months (except for one patient with suspected neurotoxoplasmosis, with an interval of 10 months between examinations); c) absence of artifacts at both imaging modalities; d) reports issued and reviewed by at least two neuroradiologists, and confirmation of the diagnostic suspicion.

Imaging parameters

MRI scans were performed in the axial plane with a 3D-GE (PRESTO) sequence, in a 3.0T magnetic field (Achieva; Philips), with 8-channel SENSE head coil. Phase and magnitude data were stored. The sequence parameters were the following: TE, 23.1 ms; repetition time (TR), 16.3 ms; flip angle, 10°; spatial resolution, $0.57 \times 0.57 \times 0.85 \text{ mm}^3$; field of view (FOV), $218 \times 218 \times 127 \text{ mm}^3$; SENSE, 2.

The CT images were acquired in a Brilliance Big Bore (Philips) apparatus in the axial plane, with the following parameters: 257 mAs/120 kV; spatial resolution, $0.39 \times 0.39 \times 5.0 \text{ mm}^3$; FOV, $199 \times 199 \times 150 \text{ mm}^3$.

SWI processing

Generally, SWIs are formed by multiplying the phase mask to the magnitude image (Figure 1). The generation of the phase mask is generated in two steps: Low frequency elimination using a high-pass filter and mask generation considering the desired phase interval. A detailed explanation about this process is below.

The filter is applied to the phase image to eliminate or attenuate the low spatial frequency components formed by the inhomogeneity of the background magnetic field (Figure 1)⁽⁶⁾. Such components are responsible for smoother

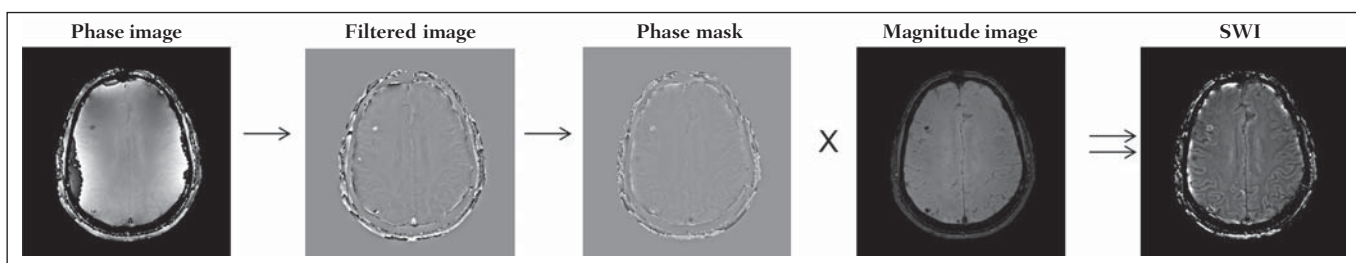


Figure 1. Diagram describing SWI processing with sigmoid mask. Patient with calcification deposit.

spatial variations on the images, thus they do not represent local variables, rather global, such as total contrast and average pixel intensity. The background magnetic field is generated by outside sources, such as, inhomogeneity of the static magnetic field (B_0) and non-uniformity of the radiofrequency field. Several types of high-pass filters can be used, here we applied a simple version as suggested by Haacke et al.⁽⁷⁾. In this case, the filtered phase image is calculated from the original complex image in the 2D k-space, truncating it in the central $n \times n$ points, adding zeros in the elements outside the truncated region and then making the subtraction of the resultant truncated phase image and the original phase image, in the real space. The window size ($n \times n$) will depend on the relation between signal-noise ratio loss on the phase image and the background field elimination, a convenient value is 64×64 considering brain images with a FOV close to 256 mm.

The phase mask generation is the most important step in SWI processing. The paramagnetic or diamagnetic contrast weighting is defined in this step. The phase image may assume only values of $-\pi$ to $+\pi$ by the Fourier transform properties and limitations of the system of MRI signal acquisition. Thus, discontinuity values of up to 2π may be observed on the phase image, in case the value exceeds such limits. Such effect is more common for long echo times, as shown on Figure 2. Such figure presents phase images with TE = 23 ms (Figure 2A) and TE = 40 ms (Figure 2B), the latter obtained by means of simulation of phase evolution from the first one. According to the equation 2 for values of susceptibility difference between hemosiderin and white matter ($\Delta\chi = 0.25 \text{ ppm}$)⁽⁸⁾, one can observe in the chart on Figure 2, that the phase difference for TE = 23 ms is approximately $-\pi/2$, and for TE = 40 ms this value should be $+\pi$. Wrap-

ping is also observed for the susceptibility difference between calcifications and white matter ($\Delta\chi = -0.15 \text{ ppm}$)⁽⁸⁾, shown on the chart: for TE = 23 ms, the phase is $\pi/2$ and for TE = 40 ms the phase is $-2\pi/3$. Thus, the phase evolved with the TE and according to the tissue susceptibility difference.

The wrapping suggests undesirable TE values for the differentiation of hemosiderin deposition and calcification lesions, depending on the magnetic field strengths. For 3T, as exemplified on Figure 2, with echo times approaching 13 and 27 ms, the phase difference in the central region of both types of lesions tend to a single value, making a correct distinction more difficult. Additionally, depending on the interval where the selected TE is situated, intensities will alternate between both types of lesions.

The phase mask is based on the linear relation between the phase evolution and the magnetic susceptibility (equation 1), valid for all the points of the image acquired in a determined magnetic field (B_0) and with a single TE. Such mask is applied to enhance the differences on the phase images on the basis of magnitude images with a more anatomical aspect of easier interpretation.

Different masks may be defined, always with values between 0 and 1 (Figure 3). A common example that is easy to be illustrated is the negative mask, assuming a unitary value for phases > 0 and from 0 to 1 for phase values in the interval $[-\pi, 0]$. Another example is the positive mask, assuming 1 for phase values < 0 and 0 to 1 for the interval $[0, \pi]$. The previous masks may be individually utilized to enhance a specific type of lesion. On the other hand, the sigmoid mask⁽⁹⁾ is more general and allows for differentiation between paramagnetic and diamagnetic tissues on a single susceptibility-weighted image. Such mask follows the behavior of the sigmoid function described on equation 3:

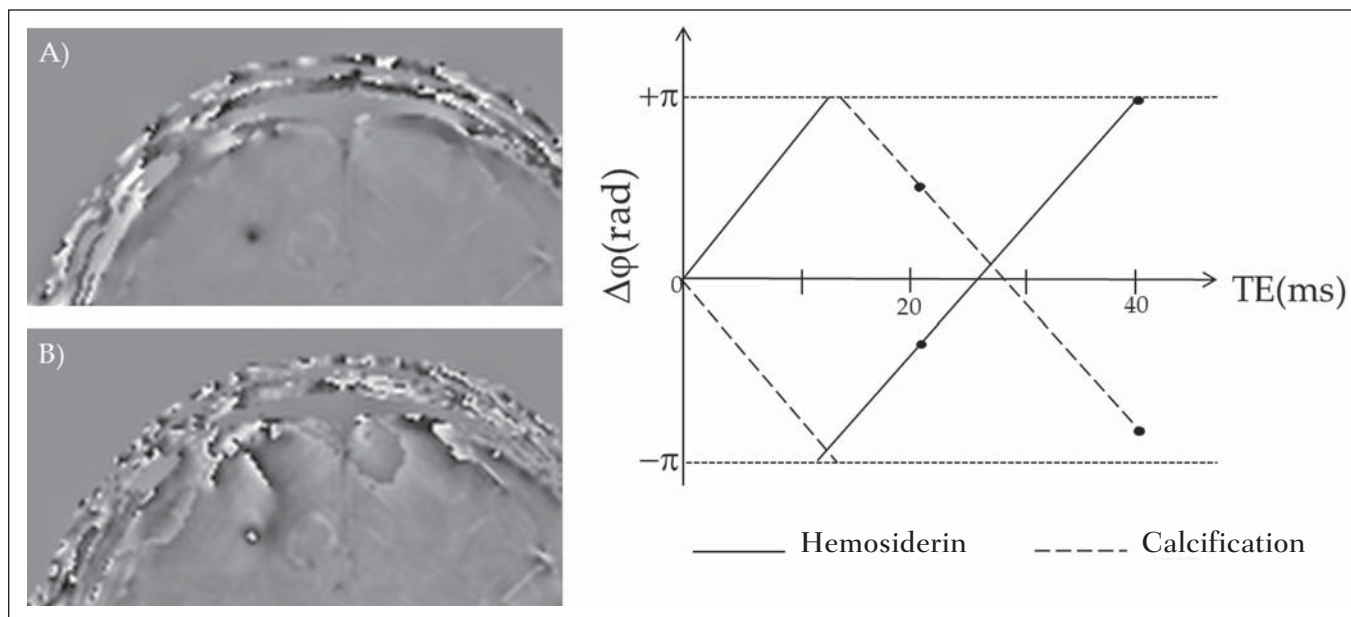


Figure 2. Wrapping effect on phase image of a patient with hemosiderin deposit. **A** and **B** phase images with TE = 23 ms and 40 ms, respectively. The chart includes phase values simulated with the “left hand” system for regions with hemosiderin and calcification deposits, considering a 3T field. The highlighted spots on the chart indicate phase values for TE = 23 ms and TE = 40 ms.

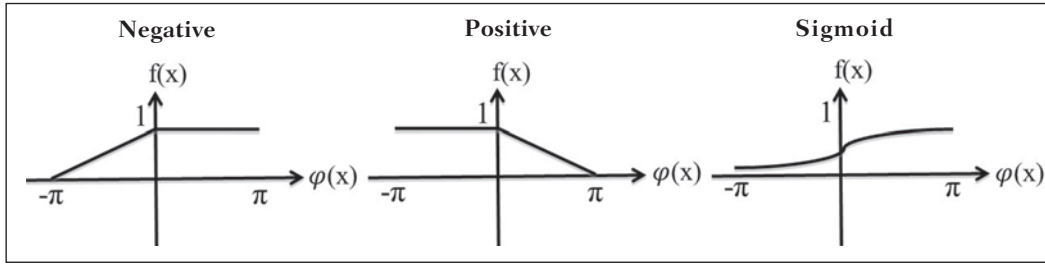


Figure 3. Phase masks defined with values between 0 and 1 according to the phase values.

$$f(r) = \frac{1}{1 + e^{(-a * (\varphi(r) - b))}} \quad (3)$$

The adjustment parameters “a” and “b” are freely selected as to achieve a good contrast-noise ratio⁽⁹⁾. In this paper, a sigmoid mask (parameters a = 0.5 and b = -0.15) was used to differentiate paramagnetic and diamagnetic tissues.

Subsequently, the phase mask is multiplied *n* times over the magnitude image to generate the susceptibility-weighted image. The number *n* of multiplications should be selected to optimize the contrast-noise ratio at SWI, as demonstrated by Reichenbach et al., such number should be close to 4⁽¹⁰⁾. Figure 4 exemplifies the change of the contrast-noise for the use of sigmoid mask multiplied 4, 6 and 8 times over the magnitude image of a patient with hemosiderin deposition.

In the present study, the SWI processing was performed in a home-made Matlab routine. In summary, a high-pass (HP) filter with window size 64 × 64⁽¹¹⁾ was selected and a sigmoid mask × 4 was applied⁽¹⁰⁾.

Effect of the spatial distribution of the phase in regions adjacent to the lesion

In addition to the punctual dependence between the phase difference and the tissue susceptibility difference, as approached by equation 1, the $\Delta\varphi(r, TE)$ is also affected in the adjacent areas, a fact that is frequently observed at the sections inferiorly and superiorly to the hemosiderin deposit or calcification (Figure 5). A more general way to write the equation 2 is to express $\Delta\varphi(r, TE)$ as a function linearly dependent of the perturbation in the main magnetic field $\Delta B(r)$ along the B_0 vector; the other components are not considered:

$$\Delta\varphi(r, TE) = \gamma * \Delta B(r) * TE \quad (4)$$

As calcification and hemosiderin deposits with spherical geometry centered at the origin are considered, the perturbation of the magnetic field at an arbitrary point resulting from such deposits might be written as follows⁽¹²⁾:

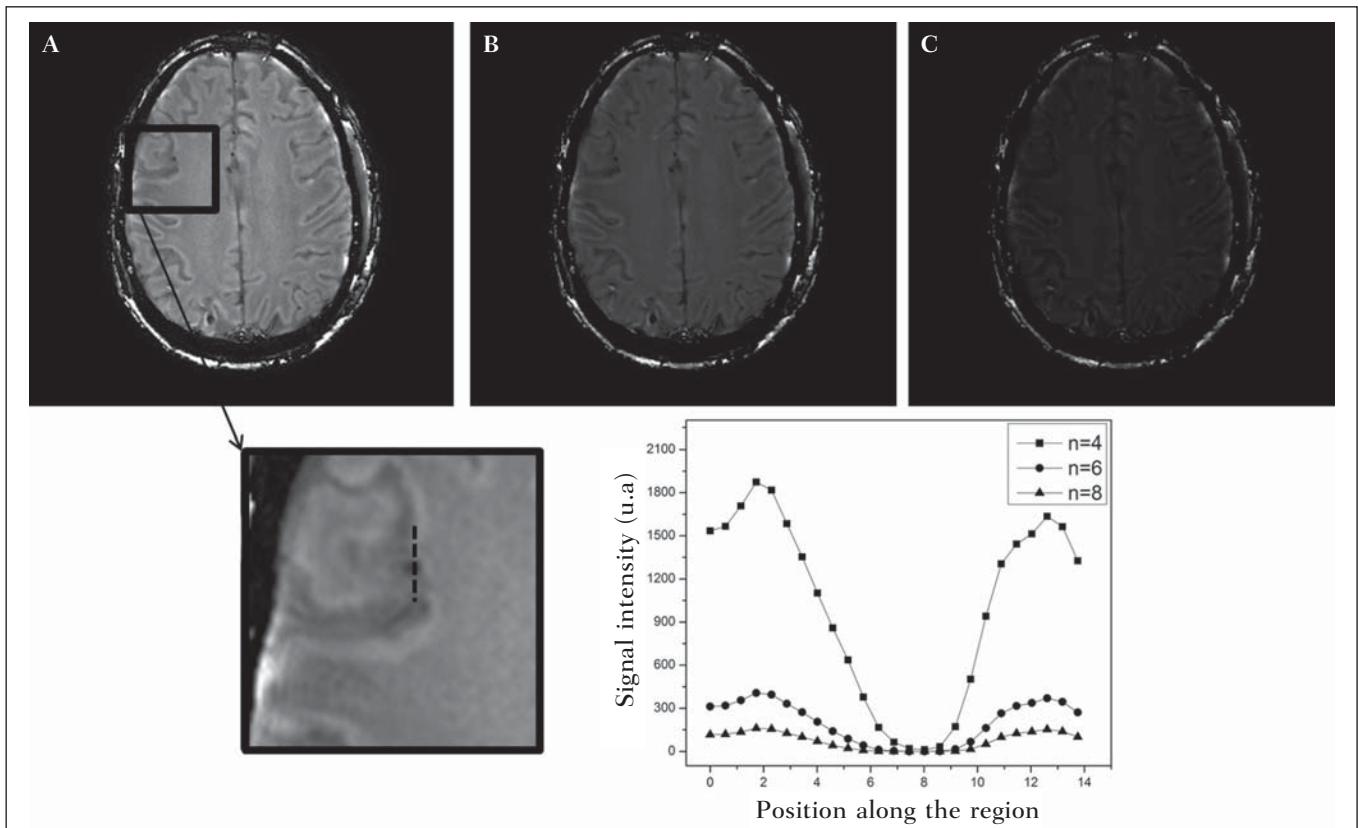


Figure 4. Susceptibility-weighted images of a patient with hemosiderin deposit (indicated with the dashed line), with different sigmoid mask multiplications **A:** *n* = 4; **B:** *n* = 6; **C:** *n* = 8. The chart includes signal intensity values for SWI along the profile indicated by the dotted line on the magnified image.

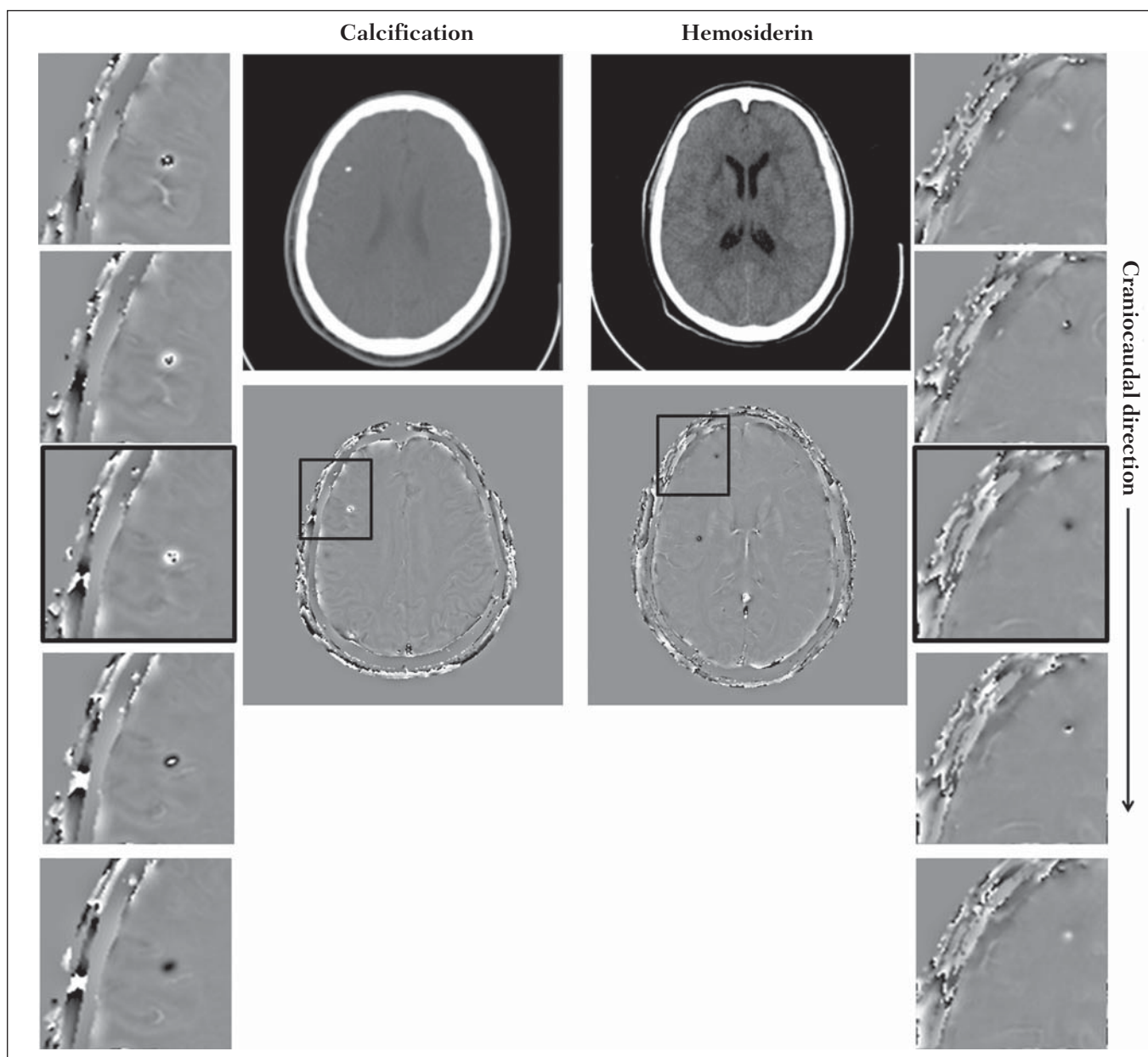


Figure 5. SWI filtered phase images (64 × 64) of a patient with calcification and other with CT-proved hemosiderin deposit. These images demonstrate the non-local of the phase evolution the on the section inferiorly and superiorly to the hemosiderin deposit and with opposite behavior for calcification and hemosiderin.

$$\Delta B(r)_{interno} = 2 * \frac{\Delta\chi(r)*B_0}{3} \quad \text{for } r \leq a \quad (5a)$$

$$\Delta B(r)_{externo} = \frac{\Delta\chi(r)*B_0}{3} \left(\frac{a}{r}\right)^3 * (3 \cos(\theta)^2 - 1) \quad \text{for } r > a \quad (5b)$$

where: a indicates the radius of the spherical lesion, and θ is the angle between the position vector (r) and the main magnetic field axis (z axis).

Using the equations 4, 5a and 5b, the authors simulated the effect of the phase evolution on the sections inferiorly and superiorly to the calcification and hemosiderin deposition with a 10 mm radius, and considering a 3T magnetic field intensity and TE = 23 ms. In such simulation, $\Delta\chi = 0.25$ ppm for hemosiderin, and $\Delta\chi = -0.20$ ppm for calcification were assumed.

RESULTS

Only four (1, 2, 3 and 4) out of the six patients presented calcifications at the CT images. For such patients, the susceptibility-weighted images presented hyperintense signal on the calcification regions (Figure 6, continuous arrows). The other two patients (5 and 6) did not present any detectable calcifications at the CT images and presented hemosiderin deposits with hypointensity at SWI (Figure 6, dotted arrows).

The HP filter failed to filter some wrapping artifacts on the SWI of the patients 2 and 4. Generally, such artifacts occurred in regions of great magnetic susceptibility difference, as the region of the nasal sinuses and ears.

Figure 7 shows the phase evolution effect inferiorly and superiorly to the radius of the simulated calcification and

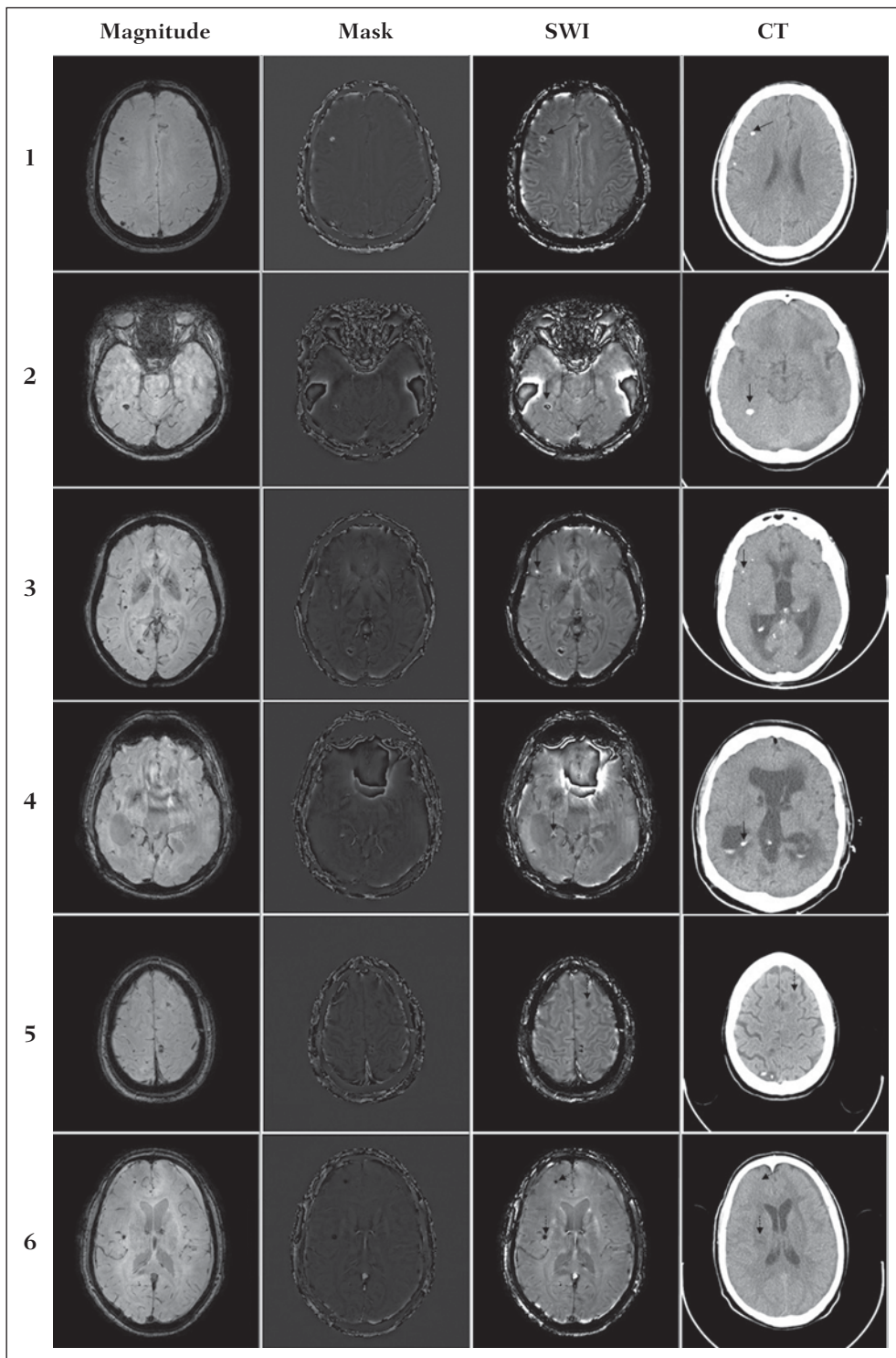


Figure 6. Magnitude, mask (multiplied 4 times), SWI and CT images on each one of the columns for all the individuals involved in the present study. The SWI processed with sigmoid mask and the respective CT image demonstrate the regions of calcification (continuous arrow) or hemosiderin (dotted arrow), depending on the case.

hemosiderin deposition. Regions outside the lesion show phase values induced by the adjacent lesion.

DISCUSSION

SWI has been suggested to identify cerebral hemosiderin and calcification deposition⁽²⁾. The proposed analysis allowed for the differentiation of such deposits by means of SWI using a sigmoid mask, and the results were validated by CT image.

Hemosiderin deposits include Fe^{+3} atoms, which are paramagnetic and distort the local magnetic field at molecular level⁽¹²⁾. The magnetic field distortion causes a different interaction between each nuclear spin of the tissue and the local magnetic field. Therefore, the phase resulting from the voxel with hemosiderin deposit evolves much more than the normal tissue in the adjacent voxel. Calcifications contain Ca^{+2} diamagnetic atoms which also distort the magnetic field leading to spins phase evolution. The phase evolution

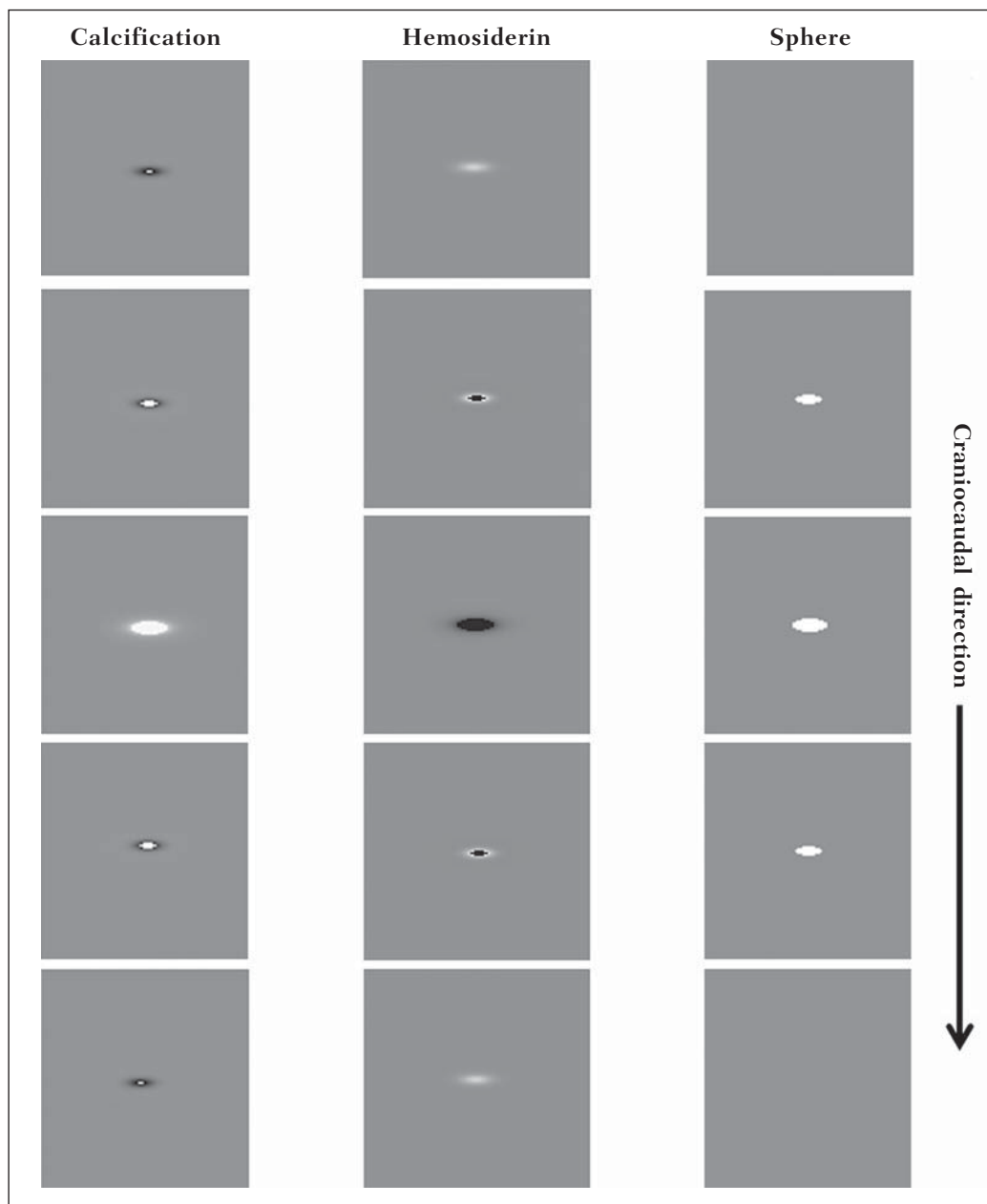


Figure 7. Image of calcification and hemosiderin deposit with spherical geometry to simulate the phase evolution effect on the sections inferiorly and superiorly to the sphere with a 10 mm-radius. 3T and TE = 23 ms were considered.

caused by the calcification occurs contrarily to Fe^{+3} deposits. Therefore, for a determined TE, it is possible to differentiate hemosiderin deposit and calcification (Figure 2).

For TE = 23 ms at 3 T the calcifications demonstrated hyperintense signal at SWI with sigmoid mask, in agreement with reports on calcifications in oligodendrogliomas, physiological lesions and cysticercosis⁽¹³⁾, and in prostate cancer⁽¹⁴⁾. SWI with longer TEs may yield results opposite to the above mentioned results. Recently, Zulfiqar et al. utilized TE = 40 ms and reported hypointense signal for calcifications in oligodendrogliomas at SWI with negative mask⁽¹⁵⁾. Additionally, they concluded that, amongst the techniques for diagnosis of cerebral calcifications by MRI, SWI was the most frequently indicated modality to detect calcifications in oligodendrogliomas with results confirmed by CT image⁽¹⁵⁾. Other authors utilized TE = 25 ms and also reported

hypointense signal for calcifications at SWI with negative mask⁽¹⁶⁾, however, the static magnetic field was less intense (1.5 T). As shown on the equation 2, the phase evolution was weaker for smaller magnetic fields. Additionally, it is important to highlight that phase images may assume opposite values as the “right hand” system is utilized. Thus, the authors point out that the results reported in the literature on this matter should be cautiously considered with a view on their application to each clinical center reality.

Also, the most MRI scanner manufacturers include the SWI sequence acquisition with automated postprocessing in their products, so the utilization of this imaging modality is increasing in the clinical practice. However, the authors highlight that the SWI is postprocessed and depends on the selection of a type of mask and some parameters which many times may be occult to radiologists. Clinical diagnoses might

be erroneously produced in the absence of knowledge about variable and/or inappropriately selected parameters.

The authors suggest a standardization of the use of SWI by a correct TE selection for the construction of a phase mask capable of enhance the contrast of both hemosiderin and calcification in order to avoid possible errors in clinical diagnoses. For example: For the acquisition, a GE sequence using TE = 23 ms for 3 T magnetic field and storing the phase and magnitude data with a reference “left-hand” system; for the SWI processing, a HP filter with a window size of 64 × 64 and using sigmoid mask with four multiplications.

The presence of magnetic susceptibility artifacts in the region of the nasal sinuses and ears of patients 2 and 4 (Figure 6) did not impair the diagnosis and differentiation between hemosiderin deposition and calcifications. In some cases, however, such artifacts prevent a complete visualization of the brain. The use of shorter TE, filter with larger window size, and other filters might remove such artifacts⁽⁸⁾.

CONCLUSION

SWI is a technique that produces postprocessed images weighting the magnetic susceptibility contrast of the phase image on the magnitude image. The TE and mask selection may change all the SWI information, affecting the diagnostic reliability. Amongst the possible masks, the authors highlight that the use of the sigmoid mask allows for enhancing the calcification and hemosiderin contrast on a single SWI.

REFERENCES

- Gupta D, Saini J, Kesavadas C, et al. Utility of susceptibility-weighted MRI in differentiating Parkinson's disease and atypical parkinsonism. *Neuroradiology*. 2010;52:1087–94.
- Berberat J, Grobholz R, Boxheimer L, et al. Differentiation between calcification and hemorrhage in brain tumors using susceptibility-weighted imaging: a pilot study. *AJR Am J Roentgenol*. 2014;202:847–50.
- Mittal S, Wu Z, Neelavalli J, et al. Susceptibility-weighted imaging: technical aspects and clinical applications, part 2. *AJNR Am J Neuroradiol*. 2009;30:232–52.
- Haacke EM, Xu Y, Cheng YC, et al. Susceptibility weighted imaging (SWI). *Magn Reson Med*. 2004;52:612–8.
- Haacke EM, Reichenbach JR. Susceptibility weighted imaging in MRI: basic concepts and clinical applications. Hoboken, NJ: Wiley-Blackwell; 2011.
- Wang Y, Yu Y, Li D, et al. Artery and vein separation using susceptibility-dependent phase in contrast-enhanced MRA. *J Magn Reson Imaging*. 2000;12:661–70.
- Haacke EM, Mittal S, Wu Z, et al. Susceptibility-weighted imaging: technical aspects and clinical applications, part 1. *AJNR Am J Neuroradiol*. 2009;30:19–30.
- Schweser F, Deistung A, Lehr BW, et al. Differentiation between diamagnetic and paramagnetic cerebral lesions based on magnetic susceptibility mapping. *Med Phys*. 2010;37:5165–78.
- Martínez Santiesteban FM, Swanson SD, Noll DC, et al. Object orientation independence of susceptibility weighted imaging by using a sigmoid-type phase window. *Proc Intl Soc Mag Reson Med*. 2006;14:2399.
- Reichenbach J, Haacke EM. High-resolution BOLD venographic imaging: a window into brain function. *NMR Biomed*. 2001;14:453–67.
- Haacke EM, Makki M, Ge Y, et al. Characterizing iron deposition in multiple sclerosis lesions using susceptibility weighted imaging. *J Magn Reson Imaging*. 2009;29:537–44.
- Schenck JF. The role of magnetic susceptibility in magnetic resonance imaging: MRI magnetic compatibility of the first and second kinds. *Med Phys*. 1996;23:815–50.
- Wu Z, Mittal S, Kish K, et al. Identification of calcification with MRI using susceptibility-weighted imaging: a case study. *J Magn Reson Imaging*. 2009;29:177–82.
- Bai Y, Wang MY, Han YH, et al. Susceptibility weighted imaging: a new tool in the diagnosis of prostate cancer and detection of prostatic calcification. *PLoS One*. 2013;8:e53237.
- Zulfiqar M, Dumrongpisutikul N, Intrapiromkul J, et al. Detection of intratumoral calcification in oligodendrogliomas by susceptibility-weighted MR imaging. *AJNR Am J Neuroradiol*. 2012;33:858–64.
- Zhu WZ, Qi JP, Zhan CJ, et al. Magnetic resonance susceptibility weighted imaging in detecting intracranial calcification and hemorrhage. *Chin Med J (Engl)*. 2008;121:2021–5.